Roman KUZIAK, Zofia KANIA, Hanna KRZTOŃ, Piotr SKUPIEŃ, Krzysztof RADWAŃSKI,
Valeriy PIDVYSOTS'KY, Artur MAZUR

Instytut Metalurgii Żelaza

ROLE OF PRECIPITATION PROCESSES IN DEVELOPMENT OF FAVOURABLE COMBINATION OF HIGH STRENGTH AND DUCTILITY OF ADVANCED BAINITIC STEELS

The paper deals with the analysis of the precipitation processes of carbo-nitrides in bainitic steels aimed at their effect on austenite microstructure evolution during thermomechanical processing and precipitation strengthening in bainitic ferrite. The commercial ThermoCalc and Prisma computer programs were used for this purpose. The investigated steels contained 0.1%C, 2%Mn, and varying content of Ti and Nb additions, including: 0.12%Ti, 0.18%Ti, 0.13%Ti + 0.035%Nb. The best effect in terms of austenite grain growth prevention and precipitation strengthening was found for the steel microalloyed with Ti alone in the amount of 0.18%.

Key words: *carbo-nitrides, precipitation strengthening, numerical modelling, bainitic steels*

ROLA PROCESÓW WYDZIELENIOWYCH W KSZTAŁTOWANIU KORZYSTNEJ KOMBINACJI WYTRZYMAŁOŚCI I CIĄGLIWOŚCI ZAAWANSOWANYCH STALI BAINITYCZNYCH

Artykuł dotyczy analizy procesów wydzielenia węglikoazotków w stalach bainitycznych wpływających na ewolucję mikrostruktury austenitu podczas obróbki cieplno-mechanicznej i umacniania wydzieleniowego ferrytu bainitycznego. Do realizacji tego celu wykorzystane zostały komercyjne programy komputerowe ThermoCalc i Prisma. Badane stale zawierały 0.1% C, 2% Mn i zmienną zawartość dodatków Ti i Nb, w tym: 0.12% Ti, 0.18% Ti, 0.13% Ti + 0.035% Nb. Najlepszy efekt w zakresie zapobiegania rozrostu ziarna austenitu i umacniania wydzieleniowego zaobserwowano dla stali mikrostopowej z dodatkiem tylko Ti w wysokości 0.18%.

Słowa kluczowe: *węgliko-azotki, umocnienia wydzieleniowe, modelowanie numeryczne, stale bainityczne*

1. INTRODUCTION

Precipitation strengthening is one of the most useful strengthening mechanisms in steel. Precipitation strengthening of polygonal ferrite has been studied intensively in recent years and the use of microalloying elements to cause the strengthening effect is a well-established technology in HSLA steels with ferrite-pearlite microstructures. Microalloying is considered as the best way of transforming standard steel into a high strength product allowing to increase yield strength by 200÷250 MPa at small microalloy additions [1–7].

For effective precipitation strengthening, it is necessary that the finely dispersed particles are precipitated in ferrite. Precipitation in polygonal ferrite can occur randomly following the austenite to ferrite transformation or by interphase precipitation characterised by the development of sheets of particles parallel to the γ/α-interface formed repeatedly with regular spacing.

Precipitation of microalloy carbonitrides during austenite to ferrite transformation occurs because the chemical driving force for this process increases suddenly and strongly as γ-phase is transformed to α-phase, reflecting the solubility drop associated with the widely different solubilities in the two phases. At low supersaturations corresponding to temperatures between A_3 and A_1 and slow cooling, the nucleation process is associated with interfaces and carbonitrides are formed repeatedly in the moving γ/α-boundary, which stands for the so called interphase precipitation. On lowering the temperature, the interface velocity increases relative to the rate of precipitation, implying that the boundary escapes the precipitates leaving supersaturated ferrite in its wake for subsequent general precipitation to occur behind the migrating γ/α-boundary. In this case, the particles are not aligned in rows but are randomly distributed and also are characterised by the occurrence of different variants of the B-N orientation relationship [7]. General precipitation occurs at temperature around 700°C and below.

For hard particles, the Ashby-Orowan mechanism (bowing of dislocations between particles) predicts that the sole parameter determining precipitation strengthening is the particle spacing and so to obtain the largest possible strengthening, the nucleation rate, which determines the density of the precipitate dispersion, should be maximised. The essential parameter governing the variation in nucleation is the chemical driving

force for M(C,N)-precipitation which depends on the available quantities of microalloying elements (M) and carbon and nitrogen.

The favourable conditions for abundant precipitation in bainitic ferrite were not previously considered for increasing strength and/or improving ductility and toughness. The reasons for this are obvious. On the one hand bainite is the most complicated microstructure of steel and there are still controversies regarding its formation. On the other hand, due to the fine scale of precipitation within bainitic ferrite it was very difficult to investigate it using conventional experimental techniques. Recent developments in thermodynamic and kinetics characterisation of phase transformation as well as an advanced metallography offer new possibilities for solving these problems. The results of "PREST" project have shown that microalloying combined with applying proper cooling routes can cause a precipitation strengthening effect increasing proof stress by 200 MPa [8].

This paper presents the results obtained within the ongoing "VirtRoll" project [9] in which precipitation strengthening of bainitic ferrite has been systematically investigated and applied for development of hot rolled bainitic strip and plate products having favourable combination of strength and ductility. Beyond this, capability of dynamic precipitation of TiC in deformed austenite to control the microstructure evolution of this phase was considered as well.

2. MATERIAL AND EXPERIMENTAL

Chemical composition of experimental steels produced at IMZ is given in Table 1. The laboratory heats having 72.5 kg were melted in VSG100 laboratory vacuum furnace and cast into slabs having dimensions: 60 × 150 × 1020 mm. The aim of the investigation was the optimization of the effect of titanium in modern bainitic steels in terms of the effect of Ti(C,N) precipitates on the kinetics of austenite restoration processes occurring during thermo-mechanical treatments, as well as precipitation strengthening effect of TiC in bainitic ferrite. Therefore, the designed steels contain high ti-

Table 1. Chemical composition of experimental steels in mas.%
Tabela 2. Skład chemiczny stali doświadczalnych w procentach masowych

Heat	Steel concept	C	Mn	Si	P	S	Nb	Ti	Mo	Al	N
S405	Bainitic low Ti	0.11	1.97	0.95	0.022	0.006	0.001	0.12	0.22	0.025	0.004
S406	Bainitic high Ti	0.11	1.95	0.98	0.020	0.007	0.001	0.18	0.20	0.022	0.004
S407	Bainitic Ti - Nb	0.12	2.00	1.01	0.02	0.008	0.035	0.13	0.20	0.019	0.004

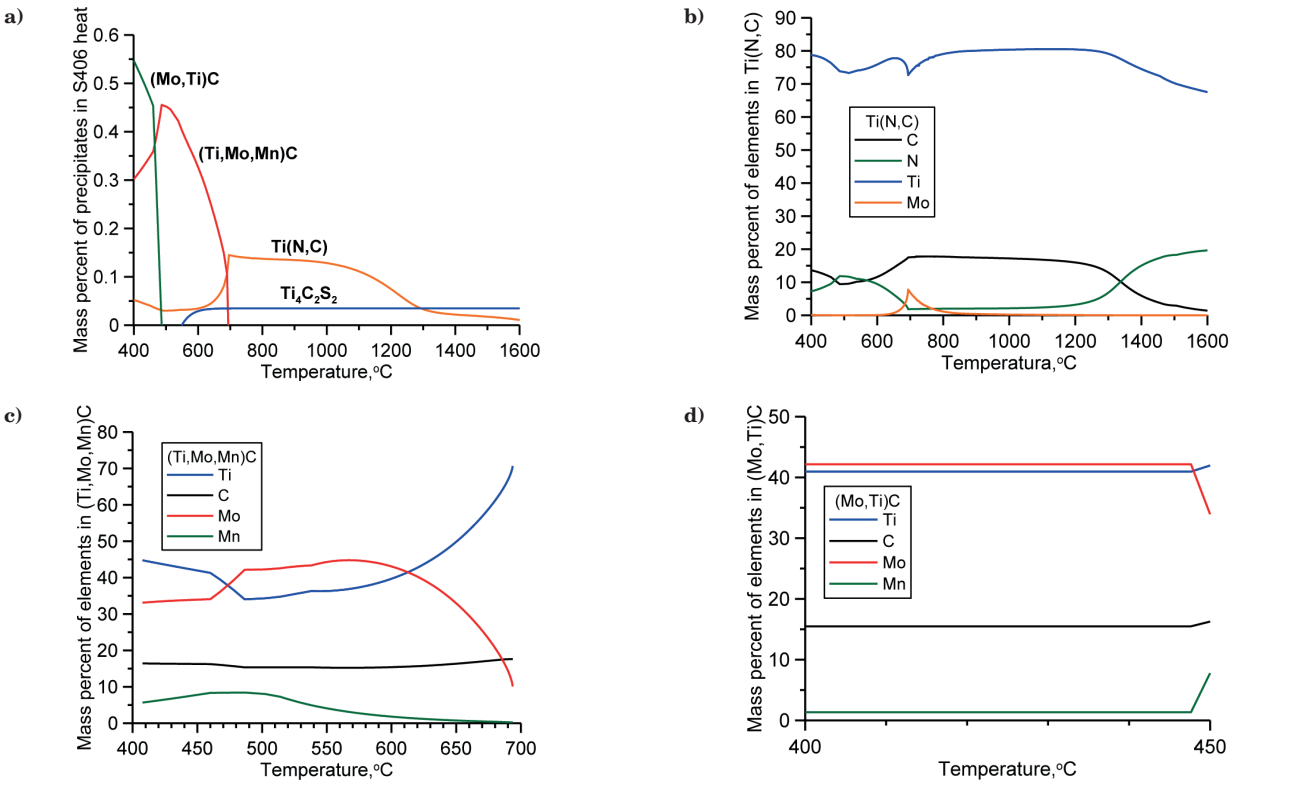

Fig. 1. Calculations of the sequence of precipitation processes in S406 steel with ThermoCalc: (a) changes of the mass percent of precipitates as function of temperature; (b) changes of the chemical composition of Ti(N,C) (c) changes of the chemical composition of (Ti,Mo,Mn)C; (d) changes of the chemical composition of (Mo,Ti)C phase. For simplicity, only main constituents were indicated in the general carbo-nitrides formulas

Rys. 1. Obliczenia sekwencji procesów wydzieleniowych w funkcji temperatury w stali S406 z wykorzystaniem programu ThermoCalc: (a) zmiana udziału wydzieleń w funkcji temperatury; (b) zmiana składu chemicznego węgliko-azotka Ti(N,C); (c) zmiana składu chemicznego węgliko-azotka (Ti,Mo,Mn)C; (d) zmiana składu chemicznego węgliko-azotka (Mo,Ti)C. W ogólnych wzorach chemicznych węglikoazotów dla uproszczenia wskazano tylko główne składniki

tanium content. The synergistic effect of combining Ti and Nb was also investigated in heat S407.

Numerical simulations of precipitation processes in investigated steels were conducted with ThermoCalc and Prisma programs. The qualitative and quantitative characterization of precipitates in experimental steel was conducted using X-ray diffraction technique, field emission gun scanning electron microscope (FEG_SEM) and transmission electron microscopy (TEM).

3. THERMODYNAMICS CALCULATIONS

ThermoCalc program was used to predict the effect of chemical composition on the sequences of precipitation processes occurring in the experimental steels [10]. The most important results are presented in figures 1-3. Heats S405 and S406 differ mainly by the titanium content. Therefore, the presentation of the results is limited to heat S406. According to calculations, at higher temperature range, carbo-sulphide $Ti_4C_2S_2$ and titanium carbo-nitride Ti(N,C) are stable, figure 1. Both phases start to form in the liquid state. The composition of carbo-sulphide is stable over the whole temperature range, whilst that of Ti(N,C) varies in the temperature range from the solidus temperature till around 1200°C and from around 800 to 600°C. The results of the calculation indicate that the composition of Ti(N,C) phase during the solidification stage is close to TiN. Decreasing the temperature causes the carbon content increase in this phase, and as a result the composition approaches that of the TiC carbide. In the temperature range from 600 to 800°C, the carbo-nitride is enriched in Mo. The thermodynamics predictions below around 700°C are uncertain, namely, they show the tendency for the formation of Mo rich carbides. This tendency, however, has not been confirmed experimentally and may be explained in terms of energetic barrier connected with the formation of Mo-enriched carbides.

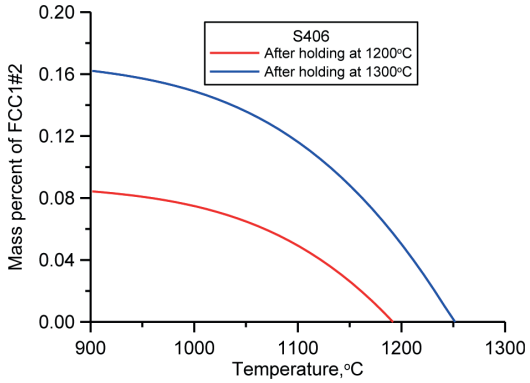

Fig. 2. Comparison of the volume fraction versus temperature changes of Ti(N,C) in S406 steel soaked at different temperatures

Rys. 2. Porównanie udziału objętościowego Ti(N,C) w funkcji temperatury w próbkach ze stali S406 wygrzewanych w różnych temperaturach

The main aim of using high titanium content in bainitic steels is to control the austenite microstructure evolution during thermomechanical processing and also to cause precipitation strengthening of bainitic ferrite matrix with TiC. Therefore, the crucial parameter to obtain the desired effect of Ti addition is the soaking temperature. Too low dissolution temperature may leave large particles of Ti(N,C) undissolved. The amount of dissolved titanium can roughly be calculated using ThermoCalc and the results of the calculations for 1200 and 1300°C are given in table 2. One can see that even applying as high temperature as 1300°C, the amount of the titanium dissolved in the austenite matrix is substantially lower than the total titanium content in the steel.

The effect of soaking temperature on the maximum amount of TiC that can precipitate during the thermomechanical processing was also calculated with ThermoCalc and is shown in figure 2. Addition of Nb in

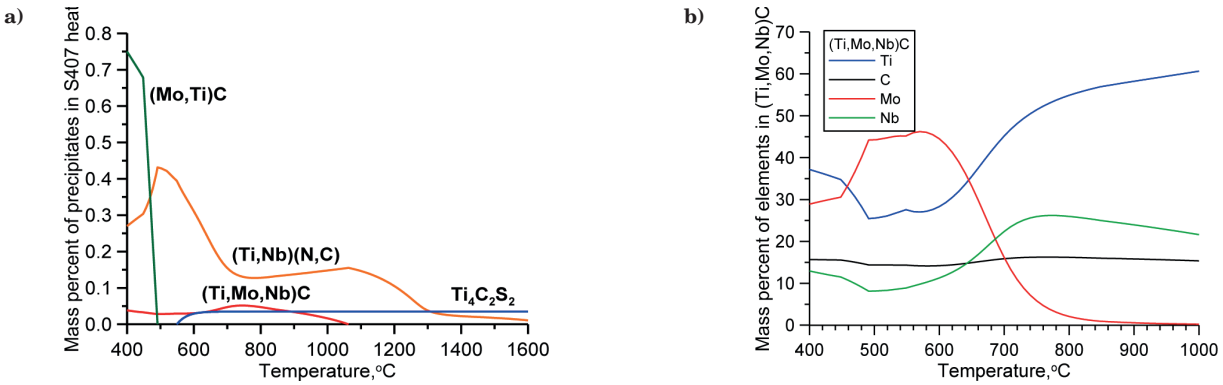

Fig. 3. Calculations of the sequence of precipitation processes in S407 steel: (a) changes of mass percent of the precipitates and (b) changes of the (Ti,Mo,Nb)C carbide chemical composition as function of temperature

Rys. 3. Obliczenia sekwencji procesów wydzieleniowych w stali S407: (a) zmiana udziału procentowego wydzieleń i (b) zmiana składu chemicznego węglika (Ti,Mo,Nb)C w funkcji temperatury

Table 2. Chemical composition of the matrix of S406 steel as a function of temperature in mas. %

Tabela 2. Skład chemiczny osnowy stali S406 w funkcji temperatury wyrażony w procentach masowych

Heat	Temperature	C	Mn	Si	P	S	Ti	Mo	N
S406	Base composition	0.112	1.95	0.98	0.020	0.007	0.180	0.200	0.004
	1300°C	0.088	1.95	0.98	0.020	0.000	0.134	0.20	0.001
	1200°C	0.074	1.95	0.98	0.02	0.000	0.070	0.20	0.000

steel S407 should change the sequence of precipitation processes, namely, below 1100°C, complex carbide (Ti-,Nb,Mo)C starts to form (Fig. 3). The first formed carbo-nitrides (Ti,Nb)(N,C) is characterized by higher Ti content compared to the Nb one. The second one is characterized by comparable Ti and Nb contents (Fig. 3b).

Due to the small sizes of the precipitates formed during the thermomechanical processing, the verification of the thermodynamic results was performed on the samples isothermally held at 450ºC for 50 hours after soaking at 1250ºC for 30 minutes. The rod's samples (7 mm in diameter and 100 mm in length) were subject

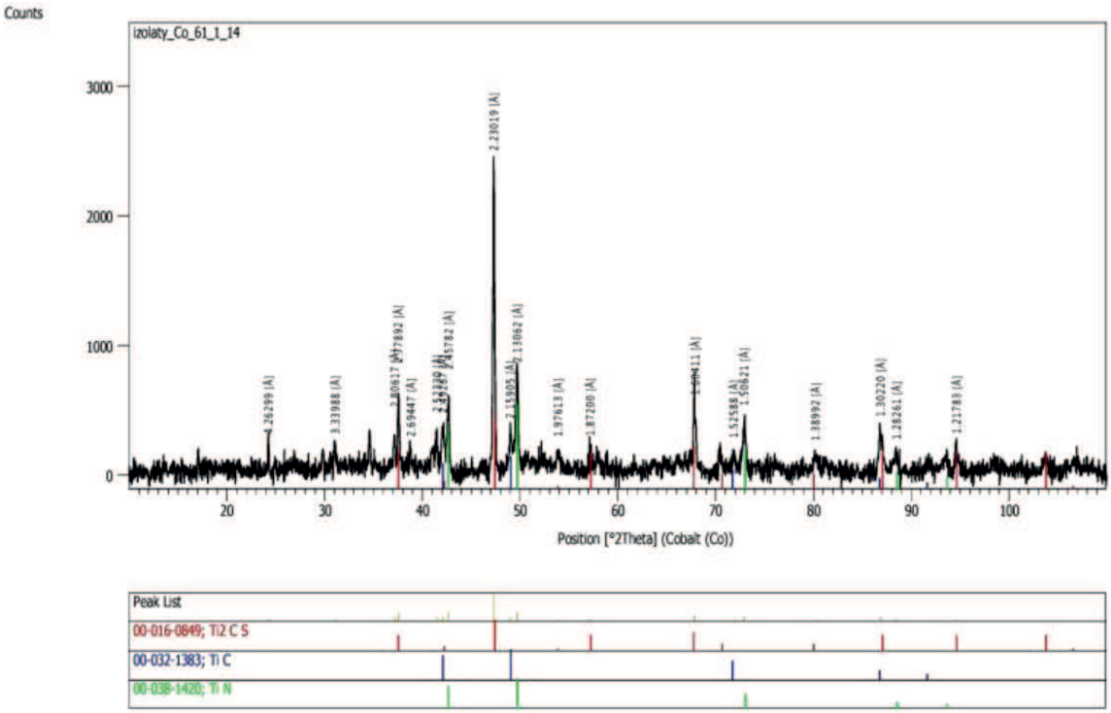

Fig. 4. X-ray diffraction pattern of residues obtained from sample of steel S406 after holding at 1250°C/8 hours followed by fast cooling to 450°C and holding for 50 hours

Rys. 4. Wyniki rentgenowskiej analizy fazowej próbek ze stali S406 po wytrzymaniu w temperaturze 1250°C/8 godzin, a następnie szybkim chłodzeniu do 450°C i wygrzewaniu przez 50 godzin

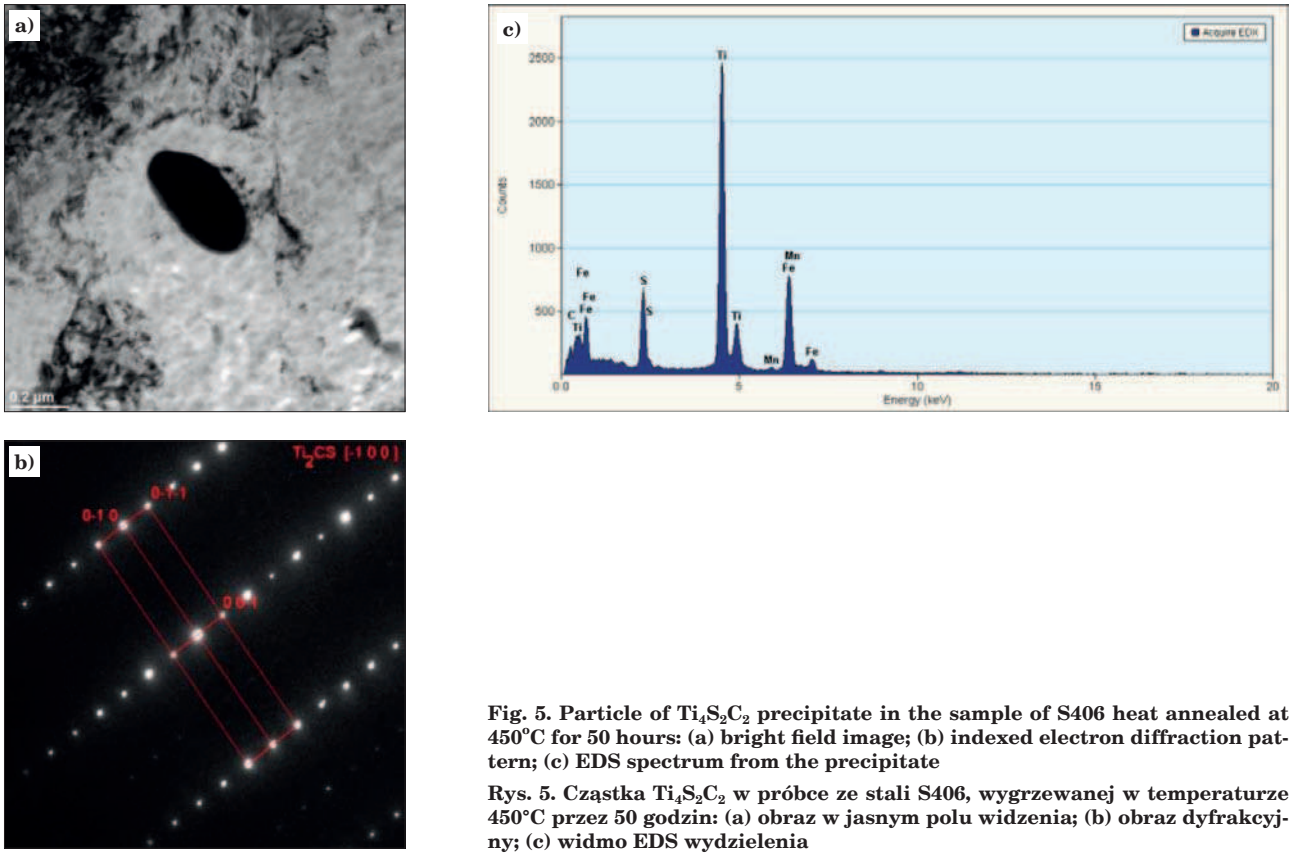

Fig. 5. Particle of $Ti_4S_2C_2$ precipitate in the sample of S406 heat annealed at 450°C for 50 hours: (a) bright field image; (b) indexed electron diffraction pattern; (c) EDS spectrum from the precipitate

Rys. 5. Cząstka $Ti_4S_2C_2$ w próbce ze stali S406, wygrzewanej w temperaturze 450°C przez 50 godzin: (a) obraz w jasnym polu widzenia; (b) obraz dyfrakcyjny; (c) widmo EDS wydzielenia

to this treatment. These dimensions allowed for fast cooling of the sample with approximate rate of 5°C/s to holding temperature. The temperature changes were monitored with thermocouple inserted in the drilled hole in the samples centre. The samples were inserted into the furnace as their temperature reached 450°C. Following this treatment, the samples were subject to electrochemical dissolution and the obtained residues were investigated by means of the X-ray diffraction method. The X-ray diffraction pattern of the residues

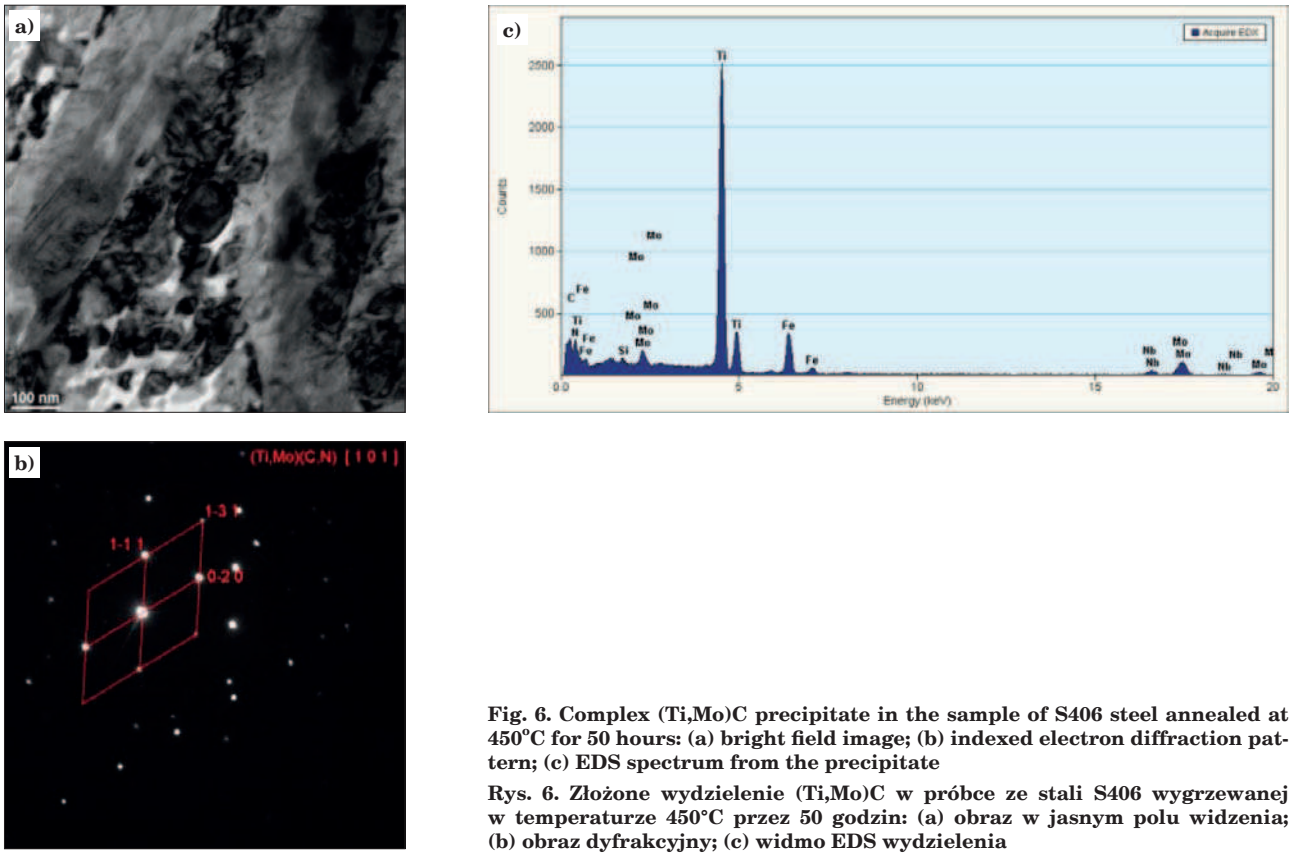

Fig. 6. Complex (Ti,Mo)C precipitate in the sample of S406 steel annealed at 450°C for 50 hours: (a) bright field image; (b) indexed electron diffraction pattern; (c) EDS spectrum from the precipitate

Rys. 6. Złożone wydzielenie (Ti,Mo)C w próbce ze stali S406 wygrzewanej w temperaturze 450°C przez 50 godzin: (a) obraz w jasnym polu widzenia; (b) obraz dyfrakcyjny; (c) widmo EDS wydzielenia

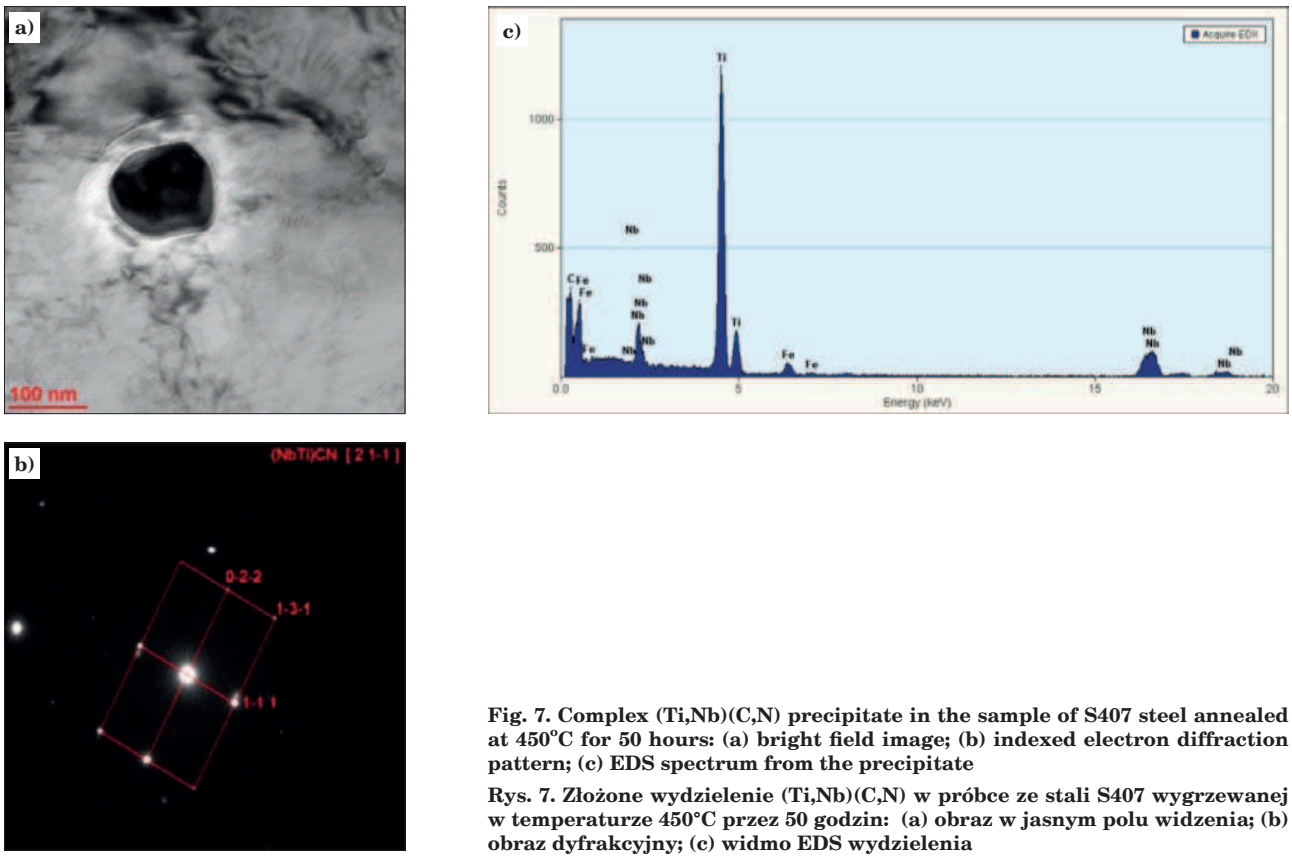

Fig. 7. Complex (Ti,Nb)(C,N) precipitate in the sample of S407 steel annealed at 450°C for 50 hours: (a) bright field image; (b) indexed electron diffraction pattern; (c) EDS spectrum from the precipitate

Rys. 7. Złożone wydzielenie (Ti,Nb)(C,N) w próbce ze stali S407 wygrzewanej w temperaturze 450°C przez 50 godzin: (a) obraz w jasnym polu widzenia; (b) obraz dyfrakcyjny; (c) widmo EDS wydzielenia

obtained from the sample from S406 steel is shown in figure 4. The sample consists of three main constituents, namely, carbo-nitride close to TiN and titanium carbide TiC and carbo-sulphide $Ti_4C_2S_2$. Both, TiN and $Ti_4C_2S_2$, were formed at higher temperatures and remained undissoved after soaking at 1250ºC (Fig. 1).

The corbo-nitride close in composition to TiN is supposed to be undissolved former Ti(N,C) complex carbo-nitride, whilst TiC precipitated during cooling and holding at 450ºC. Due to the large size, these phases are easy identifiable with TEM (Fig. 5 and 6).

In the sample of S407 heat, a complex carbide of (Ti,Nb)C was identified (Fig. 7) with the titanium as the main constituent. No carbides having high niobium content were found in the samples subject to the prolonged soaking.

4. EFFECT OF THE PRECIPITATES ON THE AUSTENITE GRAIN GROWTH CHARACTERISTICS

The capabilities of precipitates in the experimental steels to hinder the austenite grain growth during heating to temperatures of austenite stability was investigated first. The samples cut from the ingots were heated in laboratory furnace according to thermal profile shown in figure 8.

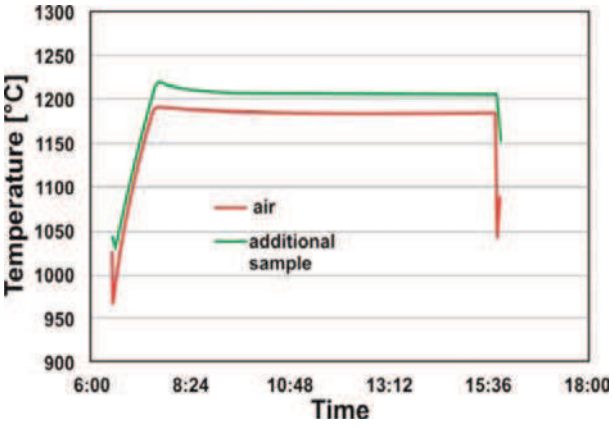

Fig. 8. Temperature changes during the heat treatment of the samples of experimental steels in the laboratory furnace

Rys. 8. Wykres zmiany temperatury podczas obróbki cieplnej próbek stali eksperymentalnych w piecu laboratoryjnym

After reaching temperature 1200°C, the samples were take out of the furnace at definite times and quenched in water. The micrographs of revealed austenite grain boundaries in the samples are shown in figure 9.

Figure 9 shows that the most stable configuration of grain boundaries is observed in the samples from heat S406. At the longest holding time at 1200°C, the sample of steel S405 are characterized by the largest austenite grain size compared to the other steels, however, the distribution of grain sizes is relatively uniform. On the contrary, the bimodal distribution of austenite grain size was developed in the sample from steel S407. This may be caused by the presence in this steel of carbo-nitrides characterized by a varying solution temperature (Fig. 3).

5. EFFECT OF THE DYNAMIC PRECIPITATION OF TIC ON THE MICROSTRUCTURAL CHANGES OCCURRING IN THE AUSTENITE DURING THERMOMECHANICAL PROCESSING

One of the aims of the current investigation is the selection of the chemical composition and processing parameters to optimize the effect of TiC precipitation and microstructural development of austenite during rolling and precipitation strengthening in bainitic ferrite. The conditions for the interaction between the microstructural changes occurring in the process of austenite deformation and dynamic precipitation were investigated first by numerical modeling with Prisma program [11]. A summary of the modeling approaches used to simulate the precipitation processes is given in [12]. The preferred nucleation on dislocation nodes was assumed in the calculation and the number of nucleation sites in unit volume was calculated with the following equation [13]:

$$N_0 = 0.5r^{1.5} \tag{1}$$

where ρ is dislocation density which can be related to the flow stress by the following equation:

$$\rho = \left(\frac{\sigma - \sigma_c}{\alpha M \mu b}\right)^2 \tag{2}$$

where: α is constant, M is Tylor factor, μ is shear modulus and b is Burgers vector.

The corrected stress – strain curves obtained in the course of plastometric investigation with Gleeble 3800 were used to calculate the dislocation density according to equation (2).

The numerical simulations showed that steel S406 exhibits the most promising characteristics of precipitation process of TiC in austenite. The results of simulations are presented in figure 10. Figure 10a shows that at all deformation temperatures, precipitation process starts shortly after deformation, however, the start of this process is delayed with respect to other deformation conditions at maximum temperature of 1100°C and the particle radius is substantially larger at this temperature compared to lower temperatures. This phenomena is related to the driving force for the precipitation effect which decreases as the deformation temperature increases. Figure 10c shows the effect of soaking temperature prior to deformation on the size of TiC precipitate. As the soaking temperature increases, the size of TiC precipitate increases which is connected to the higher amount of Ti in solid solution.

The results of numerical simulations of precipitation processes were confirmed in the course of stress relaxation investigations. Figure 11 presents the summary of the relaxation tests conducted at different deformation conditions. The effect of structure restoration processes suppression is not detected after deformation at 1100°C which is coherent with the results of numerical simulation in figure 10. On the contrary, the plateau in stress versus time curve is observed shortly after deformation at lower temperatures which is attributed to the precipitation of TiC. Deformation with low strain rates at low temperatures results in hindering the recrystallization process due to the TiC dynamic precipitation occurrence. The presence of TiC particles

in the samples subject to stress relaxation tests was confirmed by SEM (Fig. 12).

The results of the plastometric tests were used to develop the so called thermomechanical processing maps for experimental steels and examples are shown in figure 13 for strain rate 1/s. These represent the effect of strain and temperature and the following parameters relevant to the changes occurring in the austenite microstructure during rolling:

– critical strain for the dynamic recrystallization occurrence (ε_c), strain to reach the peak at the stress-strain curve (ε_p) and the strain to reach the steady state (ε_s);

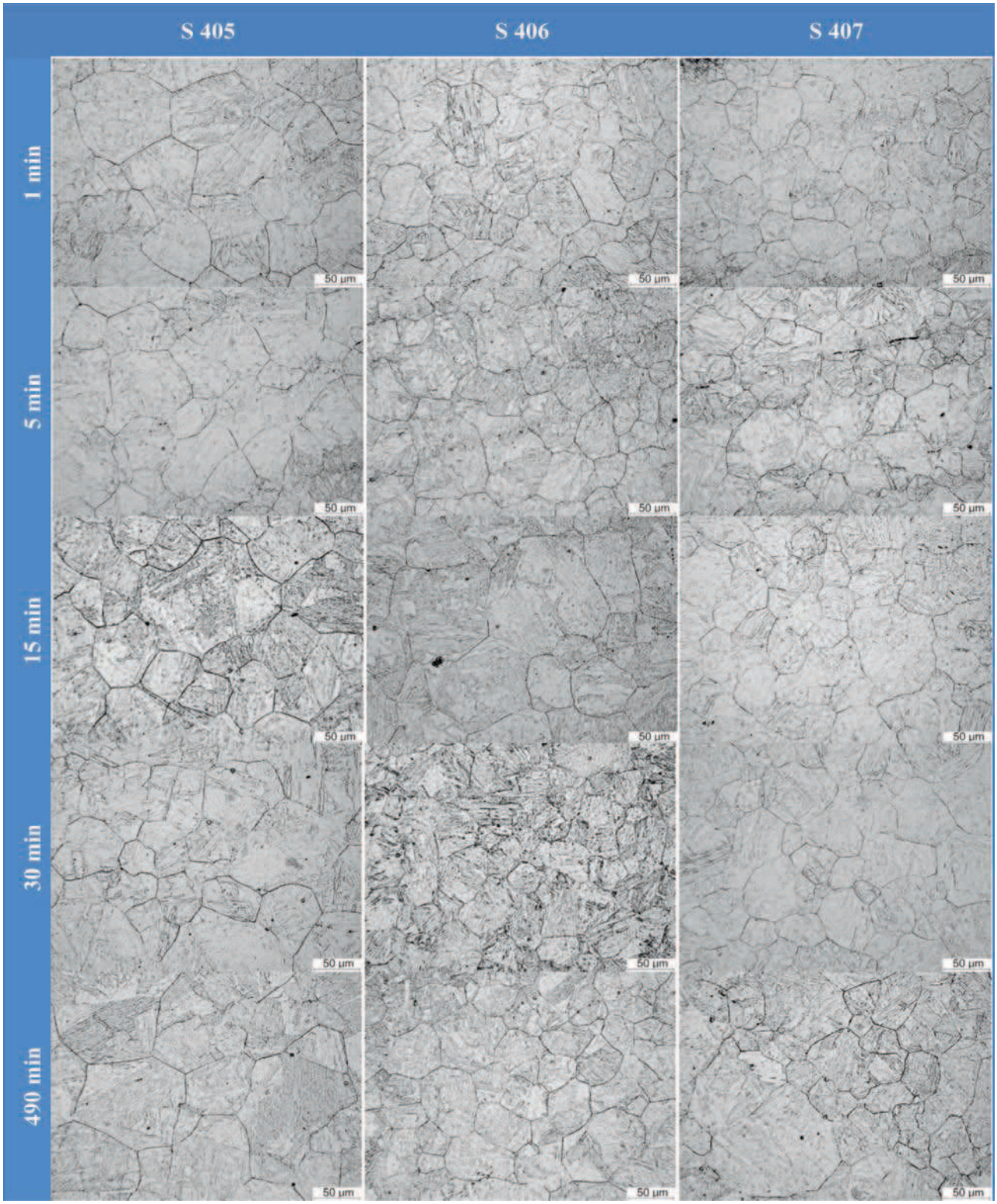

Fig. 9. Micrographs of the microstructures etched to reveal the austenite prior boundaries in the samples annealed at 1200°C for different times

Rys. 9. Zdjęcia mikrostruktury z ujawnionymi granicami ziaren byłego austenitu w próbkach wygrzewanych z różnym czasem w temperaturze 1200°C

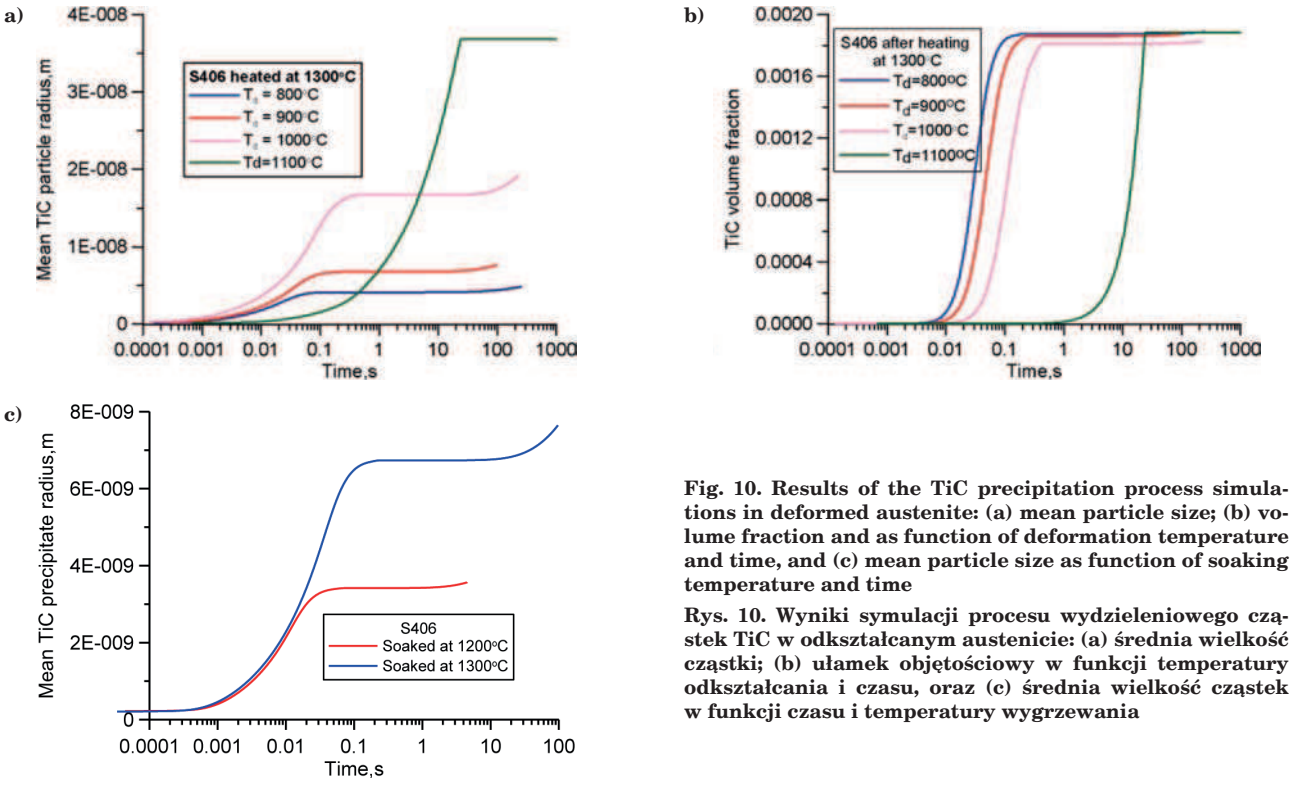

Fig. 10. Results of the TiC precipitation process simulations in deformed austenite: (a) mean particle size; (b) volume fraction and as function of deformation temperature and time, and (c) mean particle size as function of soaking temperature and time

Rys. 10. Wyniki symulacji procesu wydzieleniowego cząstek TiC w odkształcanym austenicie: (a) średnia wielkość cząstki; (b) ułamek objętościowy w funkcji temperatury odkształcania i czasu, oraz (c) średnia wielkość cząstek w funkcji czasu i temperatury wygrzewania

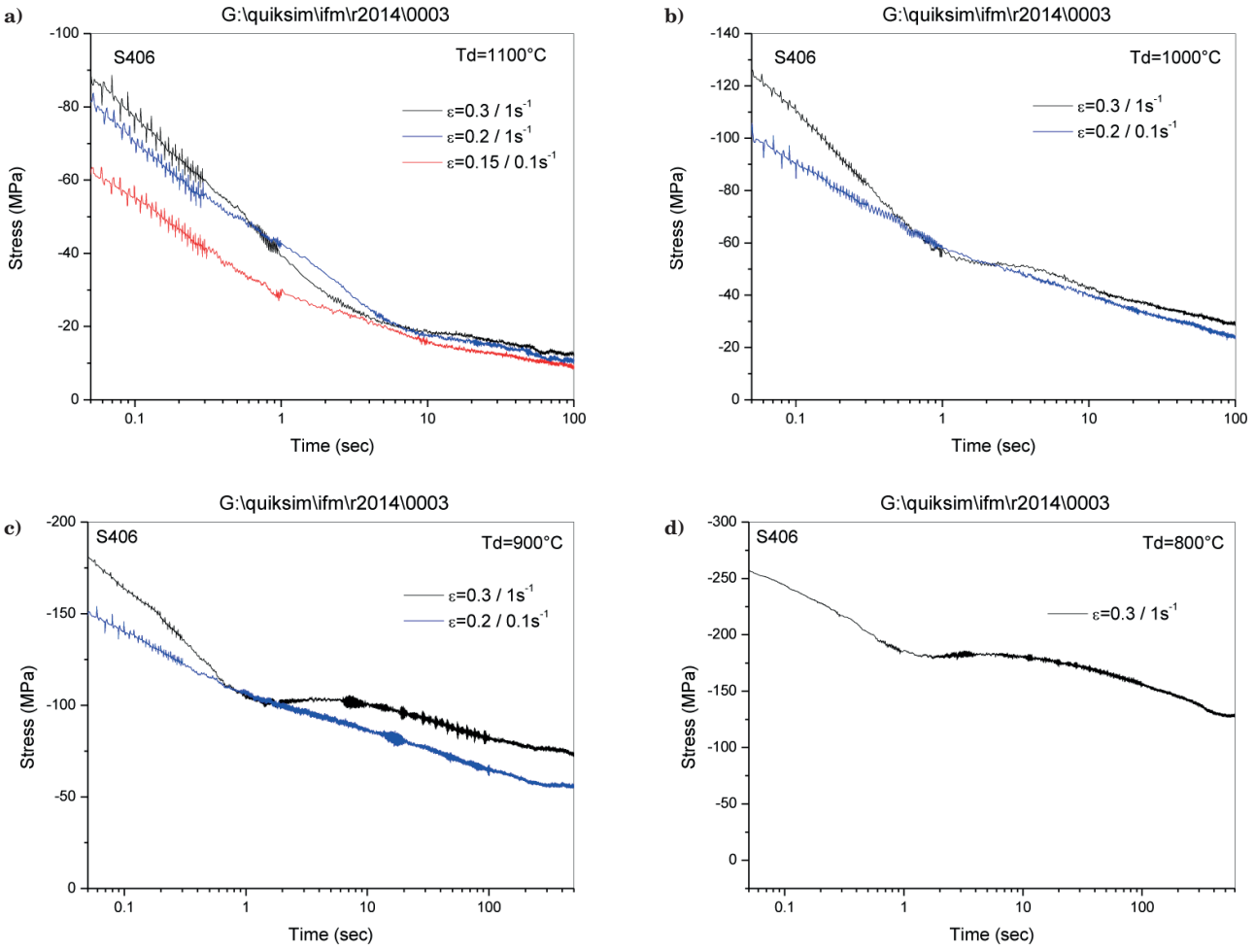

Fig. 11. Selected results of stress relaxation tests: (a) at 1100°C; (b) at 1000°C; 900°C, and (d) 800°C

Rys. 11. Wybrane wyniki badań relaksacji naprężenia: (a) w 1100°C; (b) w 1000°C; (c) w 900°C, oraz (d) 800°C

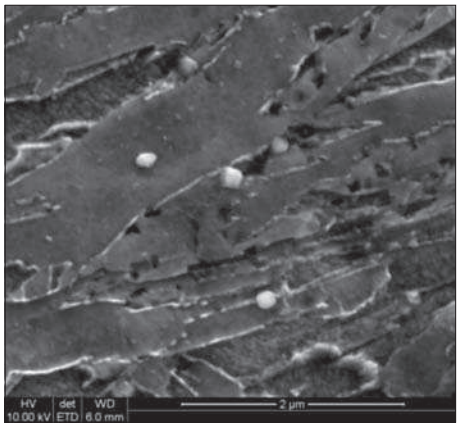

Fig. 12. TiC precipitates in the sample deformed at 1000°C to strain 0.3 and at rate 1/s after 10 seconds holding

Rys. 12. Cząstki TiC w próbce odkształconej w 1000°C z odkształceniem 0,3 i prędkością odkształcenia 1/s po 10 sekundach wytrzymania

– time to complete the static recrystallization completion;
– grain size after static, dynamic and metadynamic recrystallization.

The green contours on the graphs represent the range of deformation conditions for which the precipitation of TiC was detected with the stress relaxation technique. Analysis of the processing maps allows the conclusion that steel S406 exhibits the most stable performance with respect to the deformation conditions and at the same time finest austenite grain size after deformation.

6. THERMOMECHANICAL PROCESSING SIMULATIONS

The laboratory simulations of hot rolling were conducted using Gleeble 3800 thermomechanical simulator. Different variants were planned and executed in the plane strain conditions (Fig. 14).

Each variant involved the following stages:
– heating to soaking temperature;
– soaking;
– subjecting to deformation with different parameters;
– fast cooling to temperatures 500, 450 or 400°C followed by holding for 3600 seconds.
– slow cooling to room temperature.

The parameters of performed simulations were given in figure 15. After performing the tests, the sample was cut for the microstructure characterization and mechanical properties measurement (figure 16). Results of the mechanical properties measurement for variant 5a are summarized in figure 17.

Generally, the sample of S406 steel exhibit the best combination of strength and elongation in comparison to the other steels. This can be attributed to the highest precipitation strengthening potential of this steel as compared to the others. Microstructure of the sample of S406 steel after performed experiment is shown in figure 18.

Microstructure of the sample is composed mainly of granular and degenerated upper bainite. Allotimorphic ferrite grains are also occasionally observed in the microstructure.

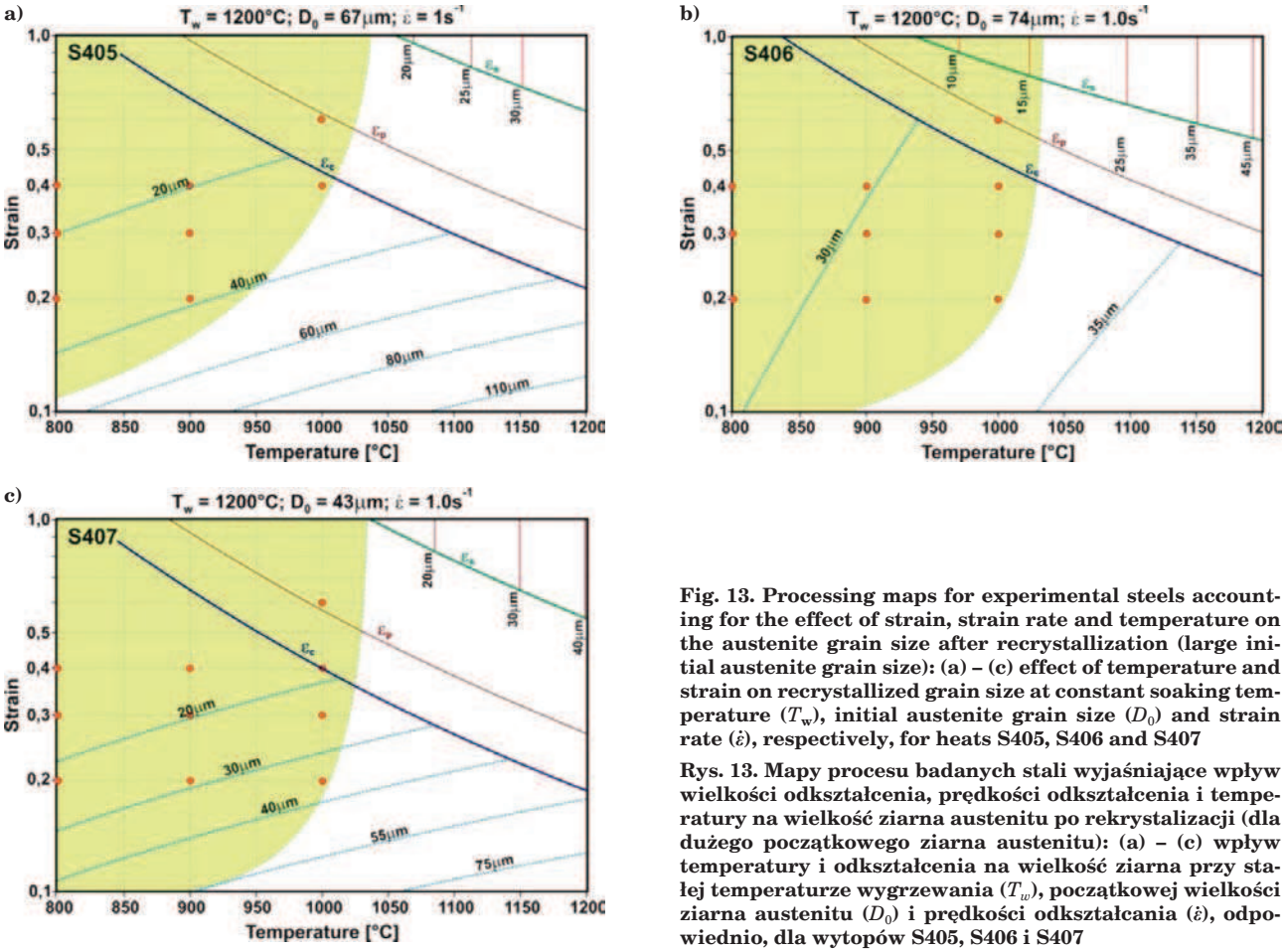

Fig. 13. Processing maps for experimental steels accounting for the effect of strain, strain rate and temperature on the austenite grain size after recrystallization (large initial austenite grain size): (a) – (c) effect of temperature and strain on recrystallized grain size at constant soaking temperature (T_w), initial austenite grain size (D_0) and strain rate ($\dot{\varepsilon}$), respectively, for heats S405, S406 and S407

Rys. 13. Mapy procesu badanych stali wyjaśniające wpływ wielkości odkształcenia, prędkości odkształcenia i temperatury na wielkość ziarna austenitu po rekrystalizacji (dla dużego początkowego ziarna austenitu): (a) – (c) wpływ temperatury i odkształcenia na wielkość ziarna przy stałej temperaturze wygrzewania (T_w), początkowej wielkości ziarna austenitu (D_0) i prędkości odkształcania ($\dot{\varepsilon}$), odpowiednio, dla wytopów S405, S406 i S407

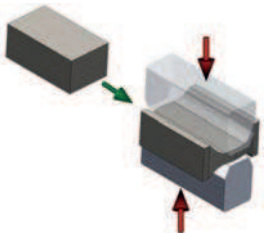

Fig. 14. Geometry of sample and schematic deformation mode of sequential plastometric tests

Rys. 14. Geometria próbki i sposób odkształcenia w badaniach sekwencyjnego odkształcenia

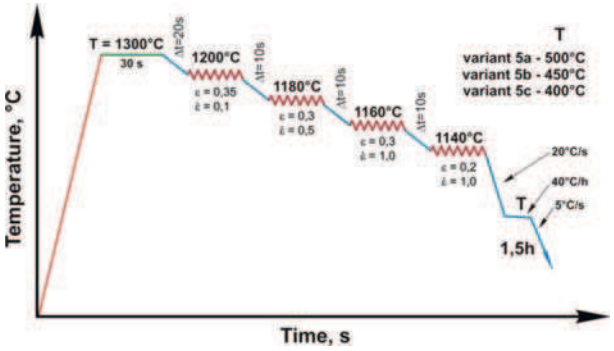

Fig. 15. Variants of the performed simulations and cooling conditions

Rys. 15. Warianty przeprowadzonych symulacji i warunków chłodzenia po odkształceniu

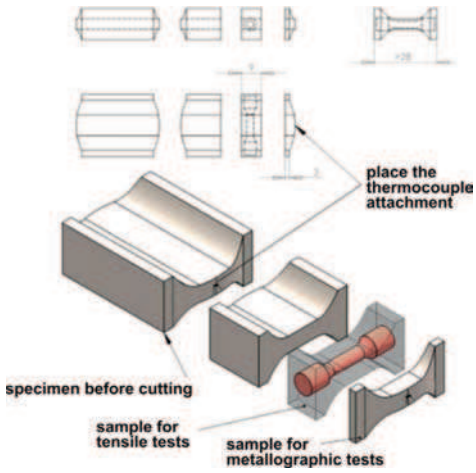

Fig. 16. Preparation of samples for metallographic examinations, hardness measurement and tensile test

Fig.16. Przygotowanie próbek do badań metalograficznych, pomiaru twardości i próby rozciągania

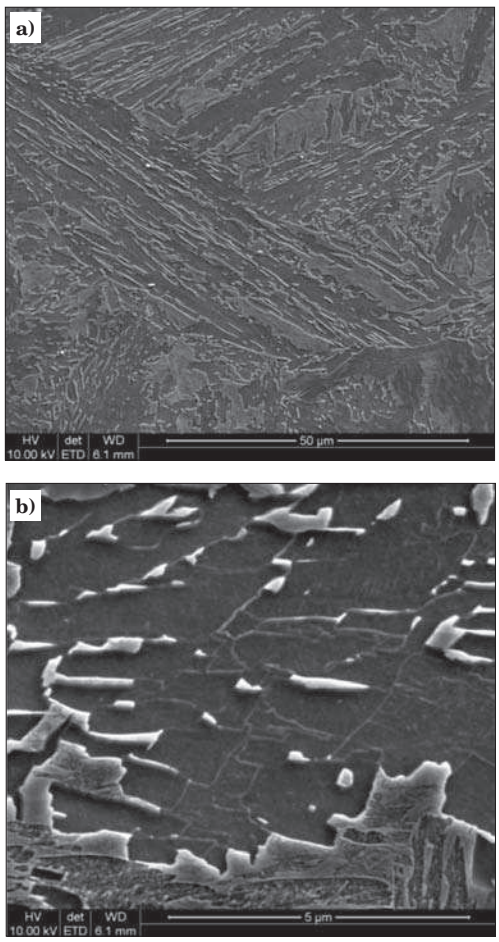

Fig. 18. Microstructure of the sample from heat S406 after variant 5a of the simulation at different magnification: a) 1000×, b) 10000×

Rys. 18. Mikrostruktura próbki z wytopu S406 po odkształceniu w płaskim stanie odkształcenia – wariant 5a przy różnych powiększeniach: a) 1000×, b) 10000×

7. PRECIPITATION STRENGTHENING IN BAINITIC FERRITE

The precipitation strengthening of baintic ferrite matrix with TiC nanoparticles was another aspect of using high titanium content in experimental steels. The precipitation process of TiC in bainitic ferrite was also simulated with Prisma program and the results are shown in figure 19. The numerical simulations

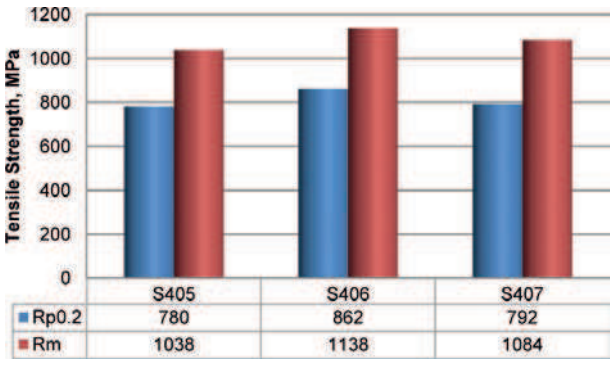

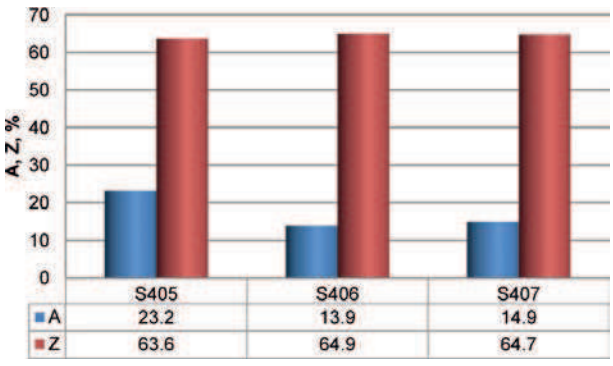

Fig. 17. Comparison of the tensile tests results for variant 5a among experimental steels

Rys. 17. Porównanie wyników testów na rozciąganie badanych stali w wariancie 5a

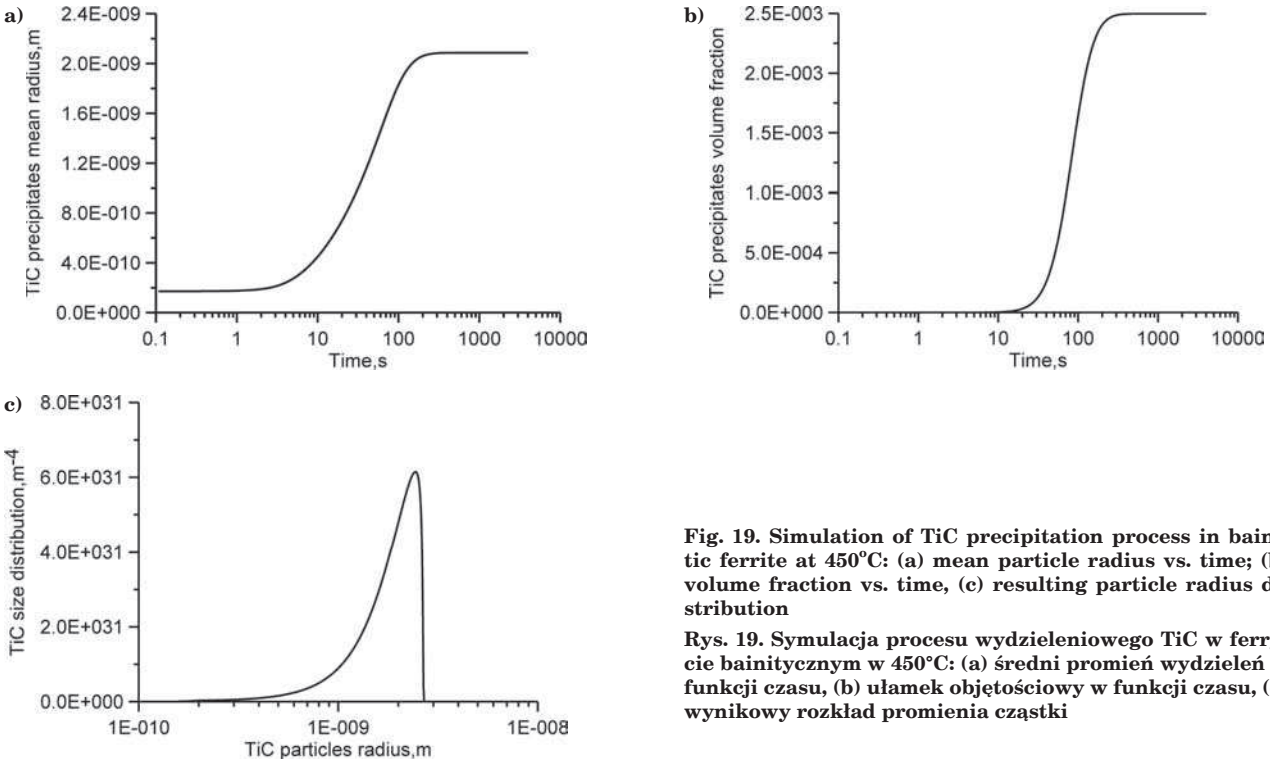

Fig. 19. Simulation of TiC precipitation process in bainitic ferrite at 450°C: (a) mean particle radius vs. time; (b) volume fraction vs. time, (c) resulting particle radius distribution

Rys. 19. Symulacja procesu wydzieleniowego TiC w ferrycie bainitycznym w 450°C: (a) średni promień wydzieleń w funkcji czasu, (b) ułamek objętościowy w funkcji czasu, (c) wynikowy rozkład promienia cząstki

show that the optimal temperature for the precipitation process is within temperature range of 400÷500°C, and holding time in the range of 100÷1000 seconds.

The TiC nanoparticles were identified with transmission electron microscopy (TEM), and an example of the results is shown in figure 20. The diameter of the precipitates is in the range 3÷5 nm which corresponds well with the results of numerical simulations.

The general approach formulated by Deschamps and Brecht was used at IMZ for the prediction of precipitation strengthening in bainitic ferrite [14]. This approach assumes that the dislocation line has to pass through all the obstacles which are encountered in the slip plane in order to cause the macroscopic strain.

Based on the results from quantitative assessments of particle size, it was assumed that the particles developed in the bainitic ferrite are relatively week and thus may be cut by dislocation. In such a case, the Friedel spacing is the appropriate measure of the mean inter-particle distance. The precipitation strengthening in such a case can be calculated with the following equation [15]:

$$\sigma_{ppt} = \frac{2M}{bLT^{1/2}}\left(\frac{K}{2}\right)^{3/2} \tag{3}$$

where: L is average interparticle spacing, T is line tension of the dislocation, M is Taylor factor, and K is the strength of the precipitate. The strength of the obstacle relative to a non-shearable precipitate is defined by the equation:

$$\Gamma = \frac{K}{2T} \tag{4}$$

where the strength of the non-shearable obstacle is $2T$ ($T = 0.5Gb^2$).

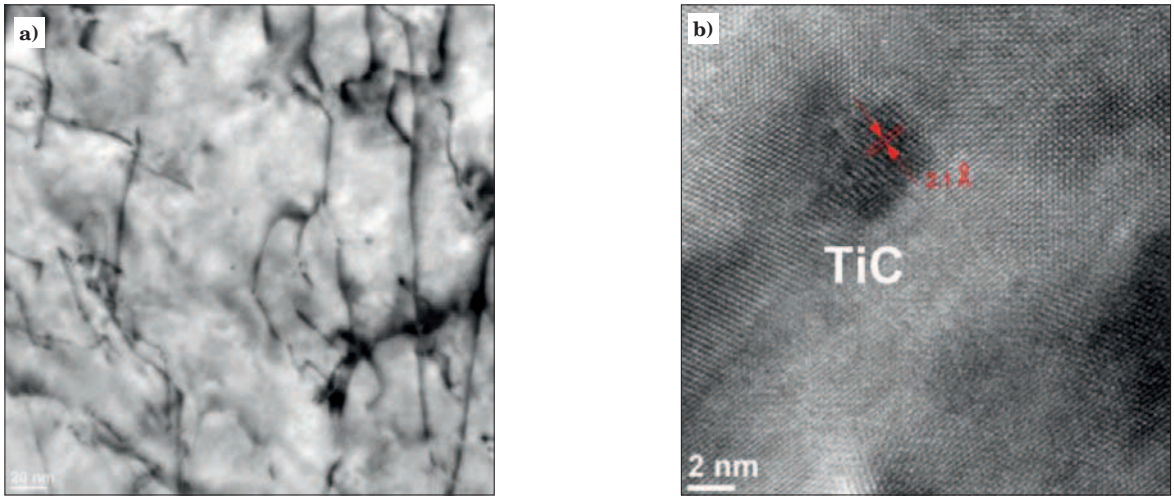

Fig. 20. Observation of TiC nanoparticles in the sample of steel S406 subject to the thermomechanical processing simulations in Gleeble 3800 according to variant 5a: (a) bright field micrograph; (b) high resolution transmission electron micrograph

Rys. 20. Obserwacja nanocząstek TiC w próbce ze stali S406 poddanej obróbce cieplno-mechanicznej w symulatorze Gleeble 3800 według wariantu 5a: (a) obraz w jasnym polu widzenia; (b) wysokorozdzielczy obraz cząstek TiC

The spacing of the plate-like precipitates on the slip plane may be calculated adopting approach described by Gladman [16]:

$$L = \frac{\pi^{1/2} D}{2f^{1/2}} \tag{5}$$

where D is the particle diameter and f is the volume fraction of precipitates.

Combining these equations, the precipitation strengthening effect of the non-shearable precipitates in the bainitic steels can be expressed as:

$$\sigma_{ppt} = \frac{2MGbf_v^{1/2}}{\pi^{1/2} D} \Gamma^{3/2} \tag{6}$$

The relative strength, Γ, of very fine (size below 5nm) NbC and TiC shearable particles was assessed by Charleux et al. [15]. The estimated value was 0.18, which means that the precipitates possessed approximately 20 pct. of the non-shearable strength. However, based upon the evaluation of the contribution of TiC particles performed in PREST project, it was assumed that the parameter Γ in equation (6) is a function of particle size and reaches value 1 when the critical size is reached by the "average" particle, figure 21.

To illustrate the performance of the present model, the precipitation process of TiC was simulated during the cooling process of a strip in the coil [8]. It was assumed that the finish rolling temperature was 850°C, and the cooling rate to the coiling temperature was 50°C/s. Different coiling temperatures, between 500 and 300°C were considered in the calculation, and the cooling rate in the coil was assumed as 40°C/hour. The calculations were stopped when the coil temperature reached 200°C. Figure 22 shows an example of the calculated particle size and number of particles in the unit of volume for 350°C coiling temperature and compares the theoretically calculated contribution of TiC with experimental values. A significant drop in the average size of the precipitates at the beginning of precipitation process is connected to the fact that a small number of precipitates is formed during the incubation time. After the incubation time, a number of small particles appears in the structure which causes the their average diameter decrease.

The results of the calculation of the contribution of precipitation strengthening with TiC to the proof stress of the strip compares well with the results of measurements.

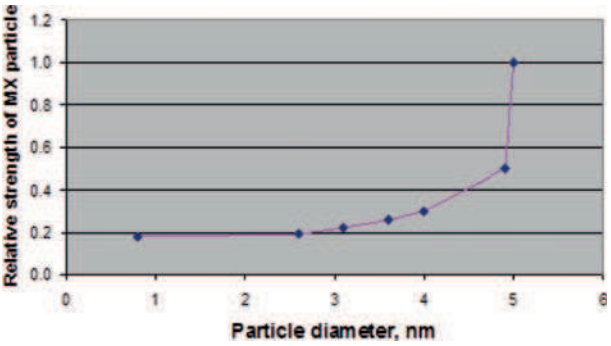

Fig. 21. Dependence of the Γ parameter on TiC particle size

Rys. 21. Zależność parametru Γ od wielkości cząstek TiC

8. CONCLUSIONS

1. The precipitation strengthening capability of TiC in bainitic ferrite was confirmed in this investigation, the assessed contribution of precipitates to proof stress of the sample form steel S406 subject to strip rolling simulation in Gleeble 3800 thermal-mechanical simulator was around 150 MPa.
2. The dynamic precipitation of TiC during thermomechanical processing was found to effectively control the evolution of austenite microstructure. It suppresses the kinetics of static recrystallization and hinders the austenite grain growth after recrystallization. The advantage of using TiC precipitation process to control the austenite microstructure evolution is mainly associated with the fact that this process leads to the grain size refinement and at the same time the grain size is not very sensitive to deformation parameters.
3. At least 0.2% of titanium should be added to the bainitic steels to obtain a required effect of TiC precipitation on austenite microstructure evolution and precipitation strengthening.
4. The calculations conducted with Prisma program and own programs developed in PREST project have shown that precipitation of TiC in bainitic ferrite is mainly controlled by Ti diffusion along dislocations produced as a result of displacive mechanism of bainitic transformation.

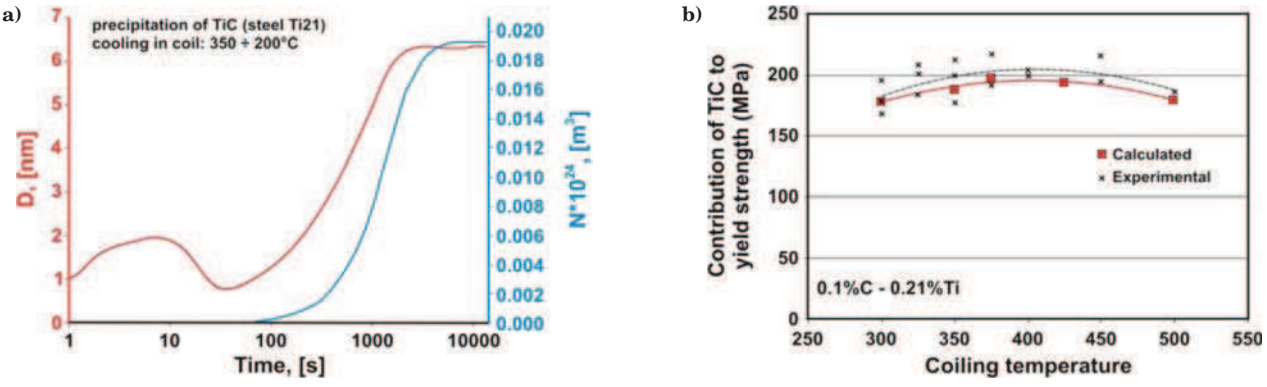

Fig. 22. Simulation of precipitation process of TiC during coiling at 350°C (a) and comparison of theoretically calculated contributions from TiC with experimental data (b)

Rys. 22. Symulacja procesu wydzieleniowego TiC podczas zwijania w krąg w temperaturze 350°C (a) i porównanie wyników teoretycznych obliczeń udziału TiC z danymi eksperymentalnymi (b)

LITERATURE

1. Zając S., Lagneborg R., Siwecki T.: The role of nitrogen in microalloying steels, Proc. Int. Conf. on "Microalloying95", Pittsburgh, 11-14 June 1995, 321
2. Parker S. V.: Property models for mixed microstructures. RFCS-project final report, 2003, p. 16
3. Mistra R., Nathani H., Hartmann J., Siciliano F.: Microstructural Evolution in a new 770 MPa hot rolled Nb-Ti microalloyed steel, Mat. Sci. Eng. A, Vol. 394 (2005), 339
4. Zając S.: Quantitative structure-property relationship for complex bainitic microstructure, RFCS Final Report, European Commision, 2005, Luxembourg
5. Senuma T.: Present status and future prospects for precipitation research in the steel industry, ISIJ Int., 42 (2002), 1
6. Jia Z., Misra R., O'Malley R., Janso S.J.: Fine-scale precipitation and mechanical properties of thin slab processed titanium-niobium bearing high strength steels, Mat. Sci. and Eng. A, 528 (2011), 7077
7. Jang J.H., Lee Ch-H., Heo Y-U, Suth D-W.: Acta Mat. 60 (2012), 208
8. Zając S.: Intense precipitaion strengthening of bainitic flat and long products, means and process routes (PREST), RFSR -CT-2004-00029
9. Kitowski J.: Virtual strip rolling Mill (VirtRoll), RFSR-CT-2013-00007
10. Lukas H. L., Fries S.G., and Sundman B.: Computational Thermodynamics: The Calphad Method. Cambridge Uni. press, 2007
11. Costa e Silva A., Nakamura L., Rizzo F.: Application of computational model ling to the kinetics of precipitation of aluminium nitride in steels, J. Min. Metall. B-Metall., Vol. 48 (2012), 471
12. Perez M., Dumont M., Acevo-Reyes D.: Implementation of classical nucleation and growth theories for precipitation; Acta Mat. Vol. 56 (2008), 2119
13. Sellars C.M., Palmiere E..: Modelling strain induced precipitation of niobium carbonitride during multipss deformation of austenite, Mat. Sci. Forum, 500-501 (November 2005), 3.
14. Deschamps A., Brechet Y.: Acta Mater.: Vol. 47, No. 1 (1999), 293
15. Charleux M., Poole W.J., Militzer M., Deschamps A.: Met. Trans. A, Vol. 32A (July 2001), 1635
16. Gladman T.: The physical metallurgy of microalloyed steels, Institute of Materials, London, 1997